Optimum aperture length for improving dispersion curve analysis in CMP Cross- Correlation of Surface Waves

Roohollah Askari*, CREWES, Department of Geoscience, University of Calgary
raskari@ucalgary.ca
and
Robert J. Ferguson, Helen Isaac, CREWES, Department of Geoscience, University of Calgary

Summary

One of the challenges of converted wave processing is to estimate a good near surface shear wave velocity model for static corrections with high lateral resolution. To this end, we have enlarged upon the idea of CMP Cross-Correlation of Surface Waves to increase lateral resolution. Our approach is fast and we believe it is more robust in the presence of variable source wavelet and noise. We cross-correlate each trace of a shot record with a reference trace that is selected from within the shot gather based on high signal to noise ratio. This step removes source effect, and converts traces to zero-phase. New midpoints that relate to the correlated traces are then calculated. We calculate the phase velocity for each CMP gather, and, we convert the resulting dispersion curve to a vertical shear wave velocity by an inverse procedure. By putting together all the vertical shear wave velocity profiles of all the CMP gathers, 2D images of shear wave velocity are obtained for the data set. In this study, we show the importance of the aperture length to precisely estimate dispersion curves and avoid modal interference. According to our results an optimum aperture length should be in the order of one to one and half the maximum wavelength observed in a record.

Introduction

Spectral Analysis of Surface Waves (SASW) (Nazarian et al., 1983) is a conventional method for the determination of 1D shear wave velocity for the near surface. The ground roll fundamental mode is analyzed by configuring and reconfiguring a pair of receivers and shots respectively. Park et al. (1999a) introduce the Multi-channel Analysis of Surface Waves (MASW) method where a dispersion curve for a multi-channel data set is estimated by transforming (e.g. the phase shift method (Park et al., 1998)) the data from the time-offset domain to the frequency-slowness (or velocity) domain. Generally speaking, in a MASW survey, the calculation of dispersion curves is faster and more accurate than those for SASW because we can isolate and distinguish other unwanted coherent event such as first arrivals, higher modes and air waves. Furthermore, MASW is less affected by ambient noise and provides a better signal to noise ratio (Hayashi and Suzuki, 2004). Therefore, MASW results in a better dispersion curve estimation, but it does at the cost of lateral resolution because of the long receiver array that must be used (Park et al., 1999b). Paradoxically, smaller arrays should be used when we need a better lateral resolution, but this reduces the resolution of the dispersion curve. Therefore, there is a tradeoff between the estimation of the dispersion curve and lateral resolution. In practice, it is critical to compensate for this tradeoff. Especially in converted wave surveys, rapid spatial velocity variations in the weathering layer need to be resolved in order to compute an appropriate velocity model for the static corrections. This requires both excellent quality phase velocity information as well as high spatial resolution.

In this study, we have enlarged upon the idea of CMP Cross-Correlation of Surface Waves (CCSW Hayashi and Suzuki, 2004) to increase lateral resolution. In the Hayashi and Suzuki's methodology, all traces within a common mid-point (CMP) are correlated with each other, traces with the same offset which belong the same CMP are stacked, and a dispersion curve is computed. Though this method

provides a good lateral resolution and dispersion curve simultaneously, the process is computationally expensive. Therefore in our approach, to reduce cost and to improve noise tolerance, we cross-correlate each trace of a shot record with a reference trace that is selected from within the shot gather based on high signal to noise ratio. This step removes the source effect, and converts traces to zero-phase. New midpoints that relate to the correlated traces are then calculated. We calculate the phase velocity for each CMP gather, and finally, the dispersion curve is converted to a vertical shear wave velocity by an inverse procedure. Putting together all the vertical shear wave velocity profiles of all the CMP gathers, a 2D image of shear wave velocity is obtained for the data set.

In this study, we use a data set acquired from a site near Priddis, Alberta, about 30 km southwest of the city of Calgary. The site of the survey is located at the eastern edge of the Rocky Mountain foothills. We show that in order to have a precise estimation of dispersion curve, the maximum relative offset which is so-called the length of aperture in this study must be the length of the maximum wavelength. Not only does our approach improve dispersion curve estimation, but, it also avoids the modal interference that is so disastrous in surface waves studies. We have obtained a 2D image of S velocity for our site. Calculated statics shows high potential for use of the method to be implemented in the static corrections for converted waves.

Theory

Assuming that a geometrical spreading correction has been applied to surface wave data, then if $h_1(t)$ is the signal recorded at station 1, and $h_2(t)$ is the recorded signal at station 2, the Fourier spectra of h_2 can be expressed as (Askari and Ferguson, 2012)

$$H_2(f) = e^{-\lambda(f)\Delta x_{1,2}} e^{-j2\pi k(f)\Delta x_{1,2}} H_1(f), \qquad (1)$$

where $H_1(f)$ are the Fourier spectra of h_1; $\lambda(f)$ is an attenuation function; $k(f)$ is a spatial wavenumber that controls wave propagation from station 1 to station 2; and $\Delta x_{1,2}=x_2-x_1$ is the distance between the two stations. For any station, such as station 3, we can write the Fourier spectra of the station (H_3) in the term of the Fourier spectra of station 1 (H_1)Therefore for any specific frequency, the spatial wavenumber between h_3 and h_2 can be obtained by

$$k(f) = -\frac{\varphi_3(f)-\varphi_2(f)}{2\pi\Delta x_{2,3}} = -\frac{\Delta\varphi(f)}{2\pi\Delta x_{2,3}}, \qquad (2)$$

where φ_2 and φ_3 are the absolute phase spectra of stations 2 and 3 respectively and $\Delta x_{2,3}=x_3-x_2$ is the distance between the two stations.

If we cross-correlate h_1 with h_2, the result is expressed in the Fourier domain as

$$C(H_1(f), H_2(f)) = e^{-\lambda(f)\Delta x_{1,2}} e^{-j2\pi k(f)\Delta x_{1,2}} H_1(f) H_1^*(f), \qquad (3)$$

where H_1^* is the complex conjugate of H_1. Similarly, we can write the Fourier spectra of the cross-correlated traces of h_1 and h_3 in the terms of the Fourier spectra of h_1 (H_1) and the relative distance between h_1 and h_3 ($x_{1,3}=x_3-x_1$). With respect to the Fourier spectra of the cross-correlated traces, the spatial wavenumber between stations 2 and 3 can be also estimated by

$$k(f) = -\frac{\emptyset_{3(f)}-\emptyset_2(f)}{2\pi\Delta x_{2,3}} = -\frac{\Delta\emptyset(f)}{2\pi\Delta x_{2,3}}, \qquad (4)$$

where $\emptyset_2$ and $\emptyset_3$ are the absolute phase spectra of the cross-correlated traces of stations 1 and 2 and stations 1 and 3 respectively. Following calculation of the wavenumber k, the phase velocity is obtained as

$$v_p = \frac{f}{k(f)}. \qquad (5)$$

We use the approach expressed in equation 3 for the calculation of the phase velocity. Because the source effect (initial phase value) is removed, therefore, the data can be sorted CMP gathers. Consequently, we calculate the phase velocity of traces in one CMP combined from different shots to

localize our analysis spatially. In this study, we use the phase shift method (Park et al. 1998) for the calculation of the phase velocity. The method is based on the estimation of the phase differences (shifts) of different traces for a range of frequencies. The method is able to estimate the phase velocity of multi-modal ground-roll (Askari et al., 2011).

Priddis Data

The data set used in this study was acquired from a site near Priddis, Alberta, about 30 km southwest of the city of Calgary. The site of the survey is located at the eastern edge of the Rocky Mountain foothills. The 3C geophones are spaced at 2m and the time sample interval is 1ms time. Vibroseis sources are spaced at 4m, with a linear sweep from 10Hz to 120Hz, and listening time at 10s.

We select the reference trace for each shot gather at an offset of 30m where the signal to noise ratio is high and wave propagation is planar (avoiding near offset effect) (Xia et al, 1999). The data are binned using a CMP bin size of 5m to increase fold so as to allow for a more stable phase velocity analysis. Figure 1 shows traces in a bin. As seen the maximum relative offset is 69m. Figure 2 shows the phase velocity that is calculated for the data in Figure 1. The maximum observed wavelength in this record is 44m. There are three distinct patches of phase velocity which are indicated by letters ‘a’, ‘b’ and ‘c’ in this image. The first approach for the estimation of a dispersion curve is to choose the patches ‘a’ and ‘b’ as the fractions of a main patch of dispersion curve because of a good apparent coherency. Applying this approach, we will end up the solid line in Figure 2 as the fundamental mode of the dispersion curve. Therefore, we have to consider patch ‘c’ as an artifact. However if we choose the patches ‘a’ and ‘c’ as the fractions of a main patch of dispersion curve (the second approach), we will end up with the dashed line in Figure 2 as the fundamental mode of the dispersion curve and therefore, we have to consider the patch ‘b’ as the first higher mode of surface wave. Though the second approach seems to be more realistic, the apparent incoherency of the patches ‘a’ and ‘c’ might make us hesitant to choose it. In order of evaluate both approaches, we shorten the aperture length (maximum relative offset) to 45m which is approximately equivalent to the maximum length of the observed wavelength and calculate the dispersion curve. Figure 3 shows the phase velocity. Here, we see two distinct patches ‘a’ and ‘b’ which the patch ‘a’ is the dispersion curve (the solid line) pertinent to the fundamental mode with a tangible coherency and patch ‘b’ is the dispersion curve (the dashed line) related to the first higher mode. It can be concluded from Figure 3, choosing an appropriate length for the aperture is a key step in CCSW analysis. It facilitate the estimation of the dispersion curves (the fundamental mode and higher modes) while maintaining a good lateral resolution. Based on this idea which is consistent with sampling theorem (Oppenheim and Schafer, 1989), we estimate the fundamental mode phase velocity for all the bins in the line. Figure 4 shows the estimated phase velocity for all the bins in the line.

Data Inversion

We can forward model dispersion curves for any geological 1D model using Knopoff’s method (Schwab and Knopoff, 1972). The Rayleigh-wave phase velocity, c_j, is determined by a nonlinear equation ‘F’ in an implicit form:

$$F(f ,c_f ,v_s ,v_p, \rho, h) = 0 \quad (j = 1, 2, \ldots ,m), \qquad (6)$$

where f is the frequency, v_s and v_p denote the S and P wave velocities respectively, h is the thicknesses of layers, ρ is the densities of the layers and, c_f is the calculated phase velocity. Using the above equation, we try to optimize a model using the method of Conjugate Gradient (Zeidouni, 2011). We calculate the dispersion function’s derivatives for a synthetic geological model (Table 1). We increase the S velocity, P velocity, and the density of the fifth layer about 20% to calculate the derivatives. Figure 4 shows the calculated derivatives for the S velocity, P velocity, and density respectively. The phase velocity is more sensitive to the variation of the S velocity. Therefore, we assume constant P velocity and density (Xia et al., 1999).

For data inversion we choose density 2300 kg/m^3 based on several logs that we have in the study area. We did not have any P velocity model for the Priddis data. Therefore, we assign an estimation of P velocity based on the S velocity and the Poisson ratio

$$V_p=V_s\left(\frac{1-\sigma}{0.5-\sigma}\right)^{\frac{1}{2}}, \quad (7)$$

where σ denotes the Poisson ratio. We repeat the inversion process for ranges of Poisson ratios from 0.4 to 0.495 which are commonly observed for the near surface (e.g. Ivanov et al., 2000). For each bin, we select the Poisson ratio which gives the best fit (less RMS error) and assign it to that bin. Figure 6 shows the predicted phase velocity (the dashed line) versus the observed phase velocity in Figure 3 (the solid line) for the poison ratio 0.495 which gives the best fit.

Figure 7 shows the S velocity model obtained from Figure 4. Some geological features at the depths 7.5m and 18m are noticeable. A channel can be seen from distance 250m to 320m. These geological features imply the high potential of CCSW for near surface imaging when an optimum aperture length is chosen. Figure 8 shows the estimated Poisson ratios versus distance for all the bins in the line. We fit a line to the Poisson ratios estimated for the line to see the trend of Poisson ratio versus CMP better. In the middle of the line, Poisson ratio drops down dramatically which suggest smallest P velocity to S velocity ratio.

Figure 9 shows the static corrections calculated from the S velocity model in Figure 7. The detailed static corrections show the high potential usage of the method for the static corrections of converted waves in multi-component studies. The relative amount of the static corrections is about 20ms which is very good for first 20m of the near surface. The reason that we are not able to image deeper layers in this study is the minimum frequency limitation. The minimum frequency that we can observe in this data set is 11Hz. This confines the depth of penetration to 20m. In practice, it is possible to increase the depth of penetration by using a low frequency source or assigning higher modes with the fundamental mode in the inversion process (Feng et al., 2005).

Conclusions

We introduce a new approach of the CMP Cross-Correlation of Surface Wave in order to obtain a better lateral resolution for near surface S velocity imaging. The idea takes advantages of SASW and MASW methods, and also is faster than the conventional CCSW (Hayashi and Suzuki, 2004) and more robust in the presence of variable source wavelet and noise. The S velocity model obtained from the method shows a good coherency to the P velocity model. This shows the potential use of the method for a better lateral resolution of S velocity imaging.

We define an optimum aperture length for maintaining lateral resolution and dispersion curves simultaneously. According to our results, the aperture length must be close to the maximum wave length. This gives us a better coherency of the fundamental mode and avoids modal interferences.

The detailed static corrections calculated from the S velocity model in this study demonstrate the high potential of the method to be utilized in seismic exploration. Surface waves provide information on the earth's layers nearest to the earth's surface. Our ability to successfully extract information from converted waves and S waves is dramatically hampered by our lack of understanding of the near-surface S-wave velocity structure. This is exactly why the surface wave methods should be taken into account by the oil and gas industry. However, if we want to obtain more reliable results from surface wave, we have to optimize acquisition parameters. In addition, in order to promote results, we should consider the limitations of surface-wave methods such as the modal superposition which can cause error in the estimation of the phase velocity.

Acknowledgements

The authors wish to express their gratitude to CREWES and its sponsors for their generous support. We express our appreciation to Dr. Robert Herrmann for providing Computer Programs in Seismology and Kevin Hall for his help during the project.

References

Askari, R., and Ferguson, R. J., 2012, Estimation Dispersion and the dissipative characteristics of surface waves in the generalized S-transform domain: Geophysics, 77, 11-20.

Askari, R., Ferguson, R. J. and K. DeMeersman, 2011, Estimation of phase and group velocities for multi-modal ground roll using the 'phase shift' and 'slant stack generalized S transform based' methods: CREWES Research Report, 23, paper 4.

Feng, S., Sugiyama, T. and Yamanaka, H., 2005, Effectiveness of multi-mode surface wave inversion in shallow engineering site investigations: Exploration Geophysics, 36, 26-33.

Hayashi, K., and H. Suzuki, 2004, CMP cross-correlation analysis of multi-channel surface-wave data: Exploration Geophysics, 35, 7–13.

Ivanov, J., C. B. Park, R. Miller, and J. Xia, 2000, Mapping Poisson's ratio of unconsolidated materials from a joint analysis of surface-wave and refraction events: Proceedings of the Symposium on the Application of Geophysics to Engineering and Environmental Problems (SAGEEP 2000), Arlington, VA, February 20–24, 11–20

Nazarian, S., K. H. Stokoe, and W. R. Hudson, 1983, Use of spectral analysis of surface waves method for determination of moduli and thickness of pavement system: Transportation Research Record, 930, 38–45.

Oppenheim, A. V., and Schafer, R. W., 1989, Discrete-Time Signal Processing. Englewood Cliffs, NJ: Prentice-Hall.

Park, C. B., R. D. Miller, and J. Xia, 1998, Imaging dispersion curves of surface waves on multi-channel record: 68th Annual International Meeting, SEG, Expanded Abstracts, 1377–1380.

Park, C. B., R. D. Miller, and J. Xia, 1999a, Multichannel analysis of surface waves: Geophysics, 64, 800–808.

Park, C. B., R. D. Miller, and J. Xia, 1999b, Multimodal analysis of high frequency surface waves: Proceedings of the Symposium on the Application of Geophysics to Engineering and Environmental Problems (SAGEEP), 115–121.

Schwab, F. A., and L. Knopoff, 1972, Fast surface wave and free mode computations, in B. A. Bolt, ed., Methods in computational physics: Academic Press, 87–180.

Xia, J., R. D. Miller, and C. B. Park, 1999, Estimation of near-surface shear-wave velocity by inversion of Rayleigh waves: Geophysics, 64, 691–700.

Zeidouni, M., 2011, Analytical and inverse models for leakage CO_2 storage: Ph.D. dissertation, University of Calgary.

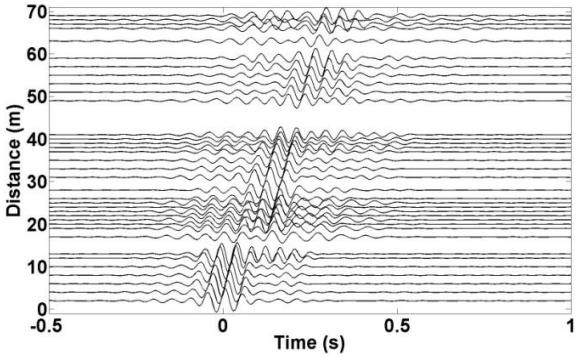

Figure 1: Traces in a bin

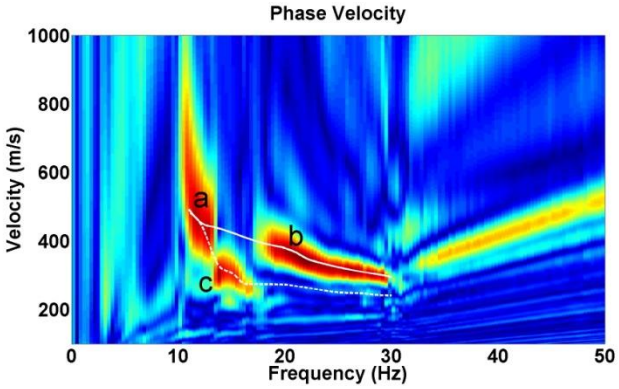

Figure 2: The phase velocity for the record in 1.

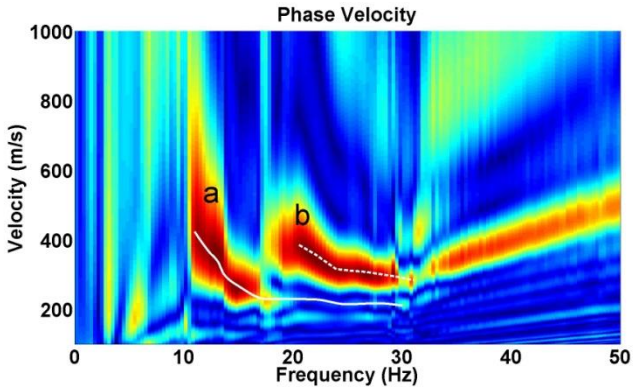

Figure 3: The phase velocity for the record in 1 with aperture length 45m. The solid line is the fundamental mode and the dashed line is the first higher mode.

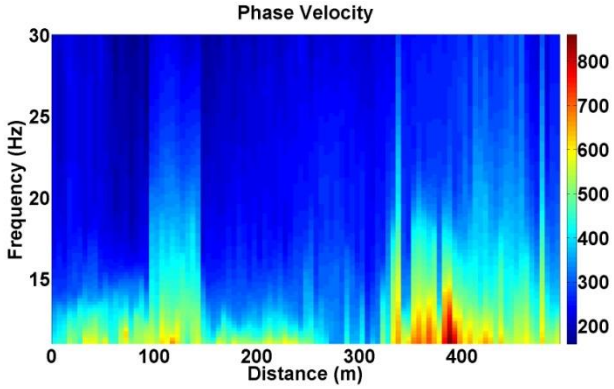

Figure 4: The estimated phase velocity for the Priddis data.

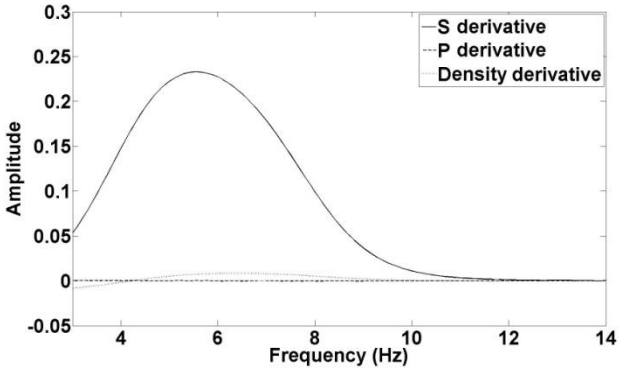

Figure 5: Phase velocity derivative with respect to S, P velocities and density respectively for the fifth layer.

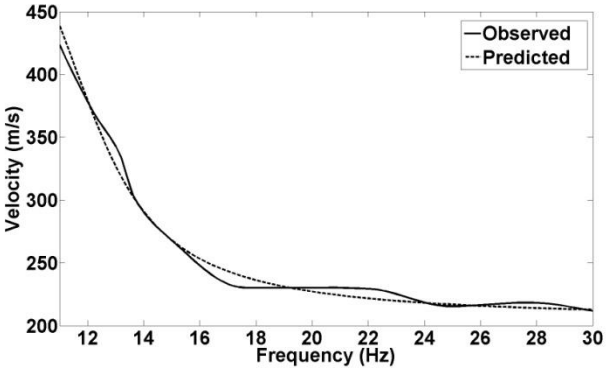

Figure 6: The predicted phase velocity (the dashed line) versus the observed phase velocity in 3 (the solid line).

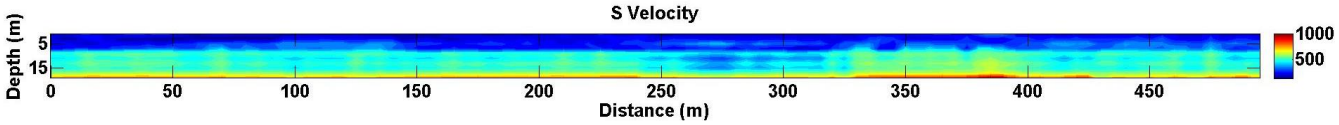

Figure 7: The S velocity model obtained from the phase velocity in 4.

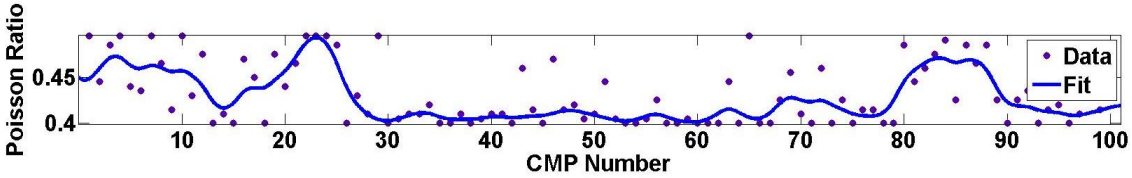

Figure 8: The estimated Poisson ratios versus distance for all the bins in the line.

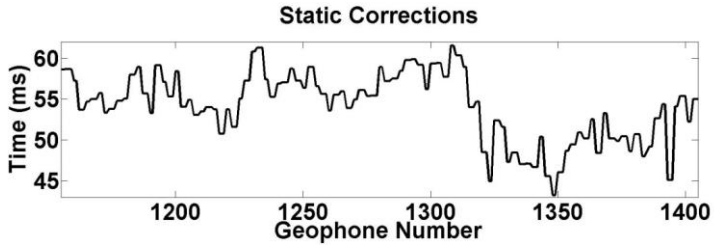

Figure 9: Static correction calculated base on the S velocity model in 7.

S Velocity	P velocity (m/s)	Density
241	1654	2000
197	1681	2000
333	1721	2000
343	1742	2000
321	1760	2000
329	1772	2000
370	1790	2000
415	1793	2000
444	1777	2000
459	1766	2000

Table 1: The geological model used for the calculation of the derivatives in Figure 5. The thickness for each layer is 5m.